



Geoarcheomorphosites under Strong Urbanization Pressure at the Tineh Plain, NE of the Nile Delta, Egypt

Maysa M. N. Taha¹ · Mansour H. Al-Hashim² · Hesham M. El-Asmar^{3,4}

Received: 16 June 2019 / Accepted: 8 January 2020 / Published online: 6 February 2020
© The European Association for Conservation of the Geological Heritage 2020

Abstract

Most geologic and geomorphologic features emerged on a deltaic plain resulted from the interplay of marine, land and river, of which are some have the potential to be a geoheritage site, this is called a geomorphosite. Over time, human impact due to settlements on the geomorphosite, reshaped and transformed the site to geoarcheomorphosite. The Great Pelusium, or Tell El-Farama, which is located along the Tineh Plain at the NE extreme of the Nile Delta between the third and fifth c. AD, is classified as a geoarcheomorphosite. The location includes several geomorphosites, such as the accreted coastal ridges, which record Late Holocene sea level changes. It also includes traces of the flash flood on the Pelusiac branch during the eighth c. AD, with the fluvial flood plain, natural levee, and crevasse splays, on which the Great Pelusium, Tell El-Luli, Tell El-Fadah, and Tell El-Makhzan were constructed. Recently, the area subjected to a hub development project, which may represent anthropogenic hazards that threaten the Great Pelusium. This study aims to quantify the potential anthropogenic hazards. The change detection shows that in 1984 the area of the geoarcheomorphosites was 424.8 km², representing approximately 67.1% of the Tineh Plain, in addition to the sand dune area of 75 km², representing 11.8%. In 2018, the area saw agricultural activities, fish farms, and an urban expansion that covered approximately 244.2 km², representing 38% of the Tineh Plain. The construction of a new hub in the Suez Canal corridor and the addition of a new community of one million people in an area of 164 km², representing 30.3% of the plain, will add more pressure on the geodiversity. A conservation plan is recommended in the form of sustainable development to save an important area of geoheritage in Egypt and convert the area into a tourism destination.

Keywords Tineh plain · Geoarcheomorphosites · Urbanization · Pelusium city

Introduction

The Nile River is the longest river in the world, flowing approximately 66,829 km from the source at Jinja in Uganda to the mouth at the Mediterranean Sea. The Nile cuts east through the Eocene plateau to El-Mokattam and west to Al-Ahram, and bifurcates north of Cairo, forming the Nile Delta (Rosetta and Damietta, Rashad and Abdel-Azeem 2010).

The Nile Delta formed in its classical shape, where the Nile River fanned out into the Mediterranean Sea. It is one of the

world's largest river deltas, extending ~240 km from Alexandria in the west to Port Said in the east and ~160 km from Cairo to north at the Mediterranean coast (Fig. 1a).

Bouriant (1900) and Butler (1996) studied the historical accounts and maps given by Herodotus (484–425 BC), Strabo (63 BC), Serapion (350 AD), and Al-Idrisi (1099–1154 AD), and mentioned that the Nile Delta branches were numerous during the Holocene; these ranged from 3 to 16. The delta fanned out eastward, as far as the old Pelusiac branch that opens at the mouth of the ancient city of Pelusium (Tell El-Farama, possibly fifth century BC) (Sneh et al. 1975), and westward, as far as the Canopic branch (Fig. 1a). The Neolithic calendar is one of the Egyptian calendars associated with the annual flood of the Nile River or the “year flooding.” The Nile covered the Egyptian land and shore with rich mud that worked as a natural fertilizer. By that time, people started to work the fields that had become fertile and, after another period, came the time for the gathering, just before the arrival of a new flood that was in rhythm with the “Nile cycle.” According to this Nile cycle, the old Egyptians arranged their agricultural rhythm according to the Egyptian life

✉ Hesham M. El-Asmar
hmelasmar@yahoo.com

¹ Department of Geology, Helwan University, Helwan, Egypt

² Department of Geology and Geophysics, King Saud University, Riyadh, Saudi Arabia

³ Vice Rectorate of Academic and Educational Affairs, King Saud University, Riyadh, Saudi Arabia

⁴ Department of Geology, Damietta University, New Damietta, Egypt

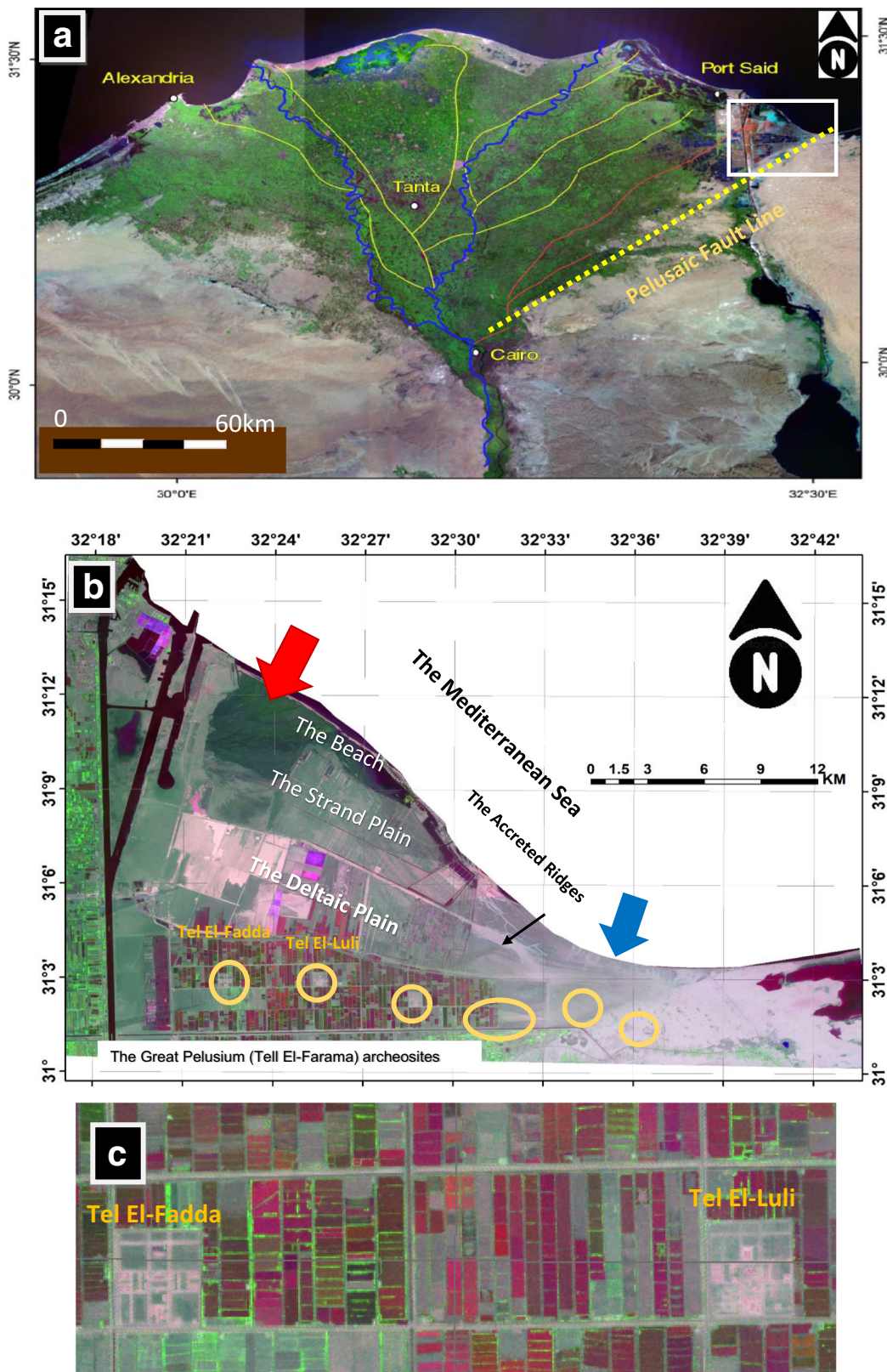


Fig. 1 Location map for the study area showing the Nile Delta with the historical Nile branches and the Tineh Plain cutting from the Nile Delta by the Suez Canal (a). Band ratio satellite image (6/7, 6/4, 4/2) showing three geomorphic units of the Tineh Plain, the beach, the strand plain, and the deltaic plain, and the archeosites (yellow circles) of the Great Pelusium

(Tell El-Farama). It also shows the Mallaha lagoon (red arrow) and the accretion ridges (blue arrow) (b). Close-up showing of how the archeosites at Tell El-Fadda and Tell El-Luli are surrounded by agricultural fields (c)

(Belen Castro 2015). Before 1900, the time when Egypt started controlling the Nile floods through several engineering structures, the annual sediment discharge averaged $160 \times 10^{12} \text{ m}^3 \text{ year}^{-1}$ (Sestini 1989), of which 100 to $115 \times 10^6 \text{ m}^3 \text{ year}^{-1}$ nourished the Nile Delta with fertile mud and reached the Mediterranean coast along the Nile branches. An amount equal to 400,000 to $3.2 \times 10^6 \text{ m}^3 \text{ year}^{-1}$, spatially distributed by longshore sediment transport, was quite adequate to maintain a reasonably stable shoreline, even with shoreline accretion (Frihy and Lawrence 2004); this left their beach ridges as records of shoreline movement (El-Asmar et al. 2015).

The Tineh Plain ($30^\circ 50' - 31^\circ 20' \text{ N}$ and $32^\circ 20' - 32^\circ 40' \text{ E}$; Fig. 1) has a triangular shape and an area of 818 km^2 . It occupies the extreme eastern part of the Nile Delta that cut from the prober delta during the excavation of the Suez Canal in 1869, making it uninhabited and far away from dense population expansion and anthropogenic activities, retaining its original geodiversity. The Tineh Plain is subdivided to three geomorphic units (Fig. 1b)—the beach, the strand plain, and the deltaic plain (Stanley and Wame 1993).

Several studies have been conducted on the geology, tectonics, and subsidence of the Tineh Plain (Sneh and Weissbrod 1973; Neev 1977; Goodfriend and Stanley 1999; Stanley 2005; Stanley et al. 2008; Stanley and Toscano 2009). The evolution of Holocene stratigraphy along the Nile Delta and the Tineh Plain was also studied (El-Asmar 1999; Quintanar et al. 2013; Pennington et al. 2017). The delta plain is composed of three subenvironments—the prodelta, the delta front, and the distributary mouth bar (Quintanar et al. 2013). The Holocene delta was a prograding one with four sedimentary members. The coastal Mb, which is made up of accreted sands, the Bilqas 2Mb, the Bilqas 1Mb, and the Modern Aeolian Mb. The Bilqas 2Mb is made up of bluish-black silty-clay to clayey-silt, containing a high percentage of organic matter related to swampy wetlands, and is thought to be deposited within the large-scale crevassing environment (Pennington et al. 2016). The Bilqas 1Mb represents a meandering environment with the characteristics uniform flood basin clays, levee silts, and channel plugs. The large-scale crevassing environments first existed near the shoreline c. 8000 cal BP, before they expanded to cover much of the delta plain for the next two or three millennia. Then, between c. 6000 and 5000 cal BP, the later and better-drained floodplain environments replaced the large-scale crevassing ones (Pennington et al. 2017). Finally, the accreted ridges formed along the Tineh Plain, representing four paleoshorelines related to Late Holocene sea level changes, and were dated back to 400–500, 1100–1200, 1400–1500, and 1700–1900 BP (El-Asmar et al. 2015).

More recently, satellite images and GIS have been used as an excellent alternative for mapping, investigating, monitoring rapid land use/land cover (LU/LC) changes, and assessing geo hazards due to anthropogenic intervention along the Tineh Plain (Kaiser 2009, El-Asmar et al. 2015; Gaber et al. 2016; Arnous et al. 2017).

By the beginning of the 1980s, the East Port Said harbor was constructed to help maintain fueling stations for ships passing through the Suez Canal waterway. From 1991, several development projects started to move eastward for the development of Sinai and the Tineh Plain. Among these projects were the cultivation and reclamation of more than 50,000 acres at the city of Pelusium (“Palouza in local Arabic”) as well as fish farming in huge areas of the Mallaha lagoon for desalinization. Besides the construction of the international coastal highway, the East Port Said harbor was updated to serve for international trading and to act as an international trading transit center, with a new industrial zone (Kaiser 2009).

Since the Suez Canal Corridor Project (SCCP) launched in 2014, the Eastern Port Said harbor authorities made plans to update the harbor, as a phase of the SCCP, into a logistic hub. This requires constructing 12-km-long docks and an industrial zone to the south of the harbor, covering 87 km^2 (approximately 10,000 acres) (EPM 2014). By 2017, the quays increased to eight, with eight stations and 8-km-long docks. By 2022, it is expected to add more four quays and create 15 stations with 16-km-long docks. In the target year 2030, the harbor will reach its full capacity with an additional ten quays for a total sum of 22. The total area of the East harbor after development is expected to be 1.5 million m^2 (approximately 17.130 acres) (Zaafarany and Alshahr 2014). Such a huge project requires conceiving of the construction of a new residential city of 13.650 acres to serve the expected moving population with capacity of approximately one million persons (GAFI 2014). Such new community creation will require expansion at the expense of the geodiversity and may threaten the archeological sites on the Tineh Plain.

The present study aims to explore the issue of deltaic geoarcheomorphosites along the Tineh Plain and to quantify the potential risk that may threaten the geodiversity resulting from urban expansion, and the expected pressure on such geoarcheomorphosites along the Tineh Plain. The study is also an attempt to enhance the awareness and the public culture toward the ways of sustainable development.

Methods

Satellite remote sensing techniques and GIS have been successfully implemented for tracing regional changes over the Earth’s surface. They have the potential to provide accurate and timely geospatial information describing certain areas of the Earth’s surface changes (Foody 2003; Herold et al. 2002; Yuan et al. 2005; El-Asmar et al. 2016). The change detection determines the application of multi-temporal data sets and quantitative analysis of the temporal change of the feature (Lu et al. 2004; Srivastava et al. 2012). Recently, LiDAR and InSAR images were successfully used for aerial and satellite archeology and detection of buried antiquities. Some results show that analyses of combined InSAR and LIDAR data on a small area can provide

an improvement in the digital elevation models (DEMs) extracted from a much larger area where only InSAR data are available (Gamba et al. 2003; Fernández et al., 2016; Monterroso-Checa 2017; Kaimaris 2018).

In the present study, two multi-temporal Landsat images (path 176, row 039) are used; one from the Multispectral Landsat 8-OLI (dated 9 August 2018) and the second collected from the Thematic Mapper TM-Landsat 5 (dated 4 August 1984). The Landsat images were free of clouds and had a spatial resolution of 30×30 m (UTM zone 36); they were acquired in 1984 from the Earth Explorer website: <https://earthexplorer.usgs.gov/>. The planet scene, in contrast, has a pixel size of 3×3 m and was acquired in 2018 from the planet imagery website <https://www.planet.com/products/planet-imagery/>. The two types of data (Landsat and planet imagery) were adequate to cover the study area. The ENVI 5.1, ERDAS, and ArcGIS 10.3 software were utilized in this research.

A DEM (ASTER, 30-m resolution) of the Tineh Plain was used to detect the elevation profile of the study area. Atmospheric correction of all Landsat imagery was done using the FLAASH (fast line-of-sight atmospheric adjustment of spectral hyper cubes) model (ENVI 2009) to correct for atmospheric effects. By applying the FLAASH model, the wavelengths were corrected in the visible through the near-infrared (NIR) and short-wave infrared (SWIR) ranges (Yuan and Niu 2008).

Image enhancement techniques were used in the present study to improve the clarity of LU/LC changes by increasing the apparent distinction between the features resulted from different activities along the El-Tina plain. Enhancement techniques occur either as pixel-to-pixel or post-classification comparisons (Mather 1999; Shalaby and Tateishi 2007).

Image classification is a widely used technique for extracting the target thematic information. In the present study, a LU/LC map was designed using an Iterative Self-Organizing Data Analysis Technique (ISODATA); an unsupervised classification (ERDAS 2005) of the full data set was performed on the Tineh Plain using optical data (1984 and 2018). The priority of this classification type is that users do not need to know the number of image clusters. A computer runs the algorithm through many iterations until a threshold is reached; each spectral class was then assigned to a particular piece of land (Memarsadeghi et al. 2007).

Band ratios are mathematical relationships between different bands of satellite images that enable investigations on the intensity and distribution in a semi-quantitative way for a specific emission or absorption feature (Drury 2001). Band rationing resulted from dividing the DN values of one band by the corresponding DN values of another band. The derived DN ratios are then displayed as a grayscale image (Sabins 1997). Landsat 8 band ratios (6/7, 6/4, 4/2) have been performed for accurate distinguishing and mapping of the different landforms on the Tineh Plain.

Image difference was used for change analysis with imagery that describes the same area at different times. With image difference, you can highlight specific areas of change in whatever amount you choose. Two images are generated from image-to-image comparison; one is the difference grayscale image and the second is a five-class thematic image ERDAS (2005). Hussain et al. (2013) and Chen et al. (2018) used a similar change detection method. The difference grayscale image, composed of single-band continuous data, resulted from the subtraction of the two selected images. Because image difference calculates change in brightness values over time, the difference image simply reflects that change using a grayscale image. Brighter areas have increased in reflectance; this may mean clearing of forested areas. Dark areas have decreased in reflectance; this may mean an area has become more vegetated, or the area was dry and is now wet. The highlight difference image divides the changes into three categories: decreased, unchanged, and increased. The decreased class represents areas of negative (darker) change greater than the threshold for change and is red in color. The increased class shows areas of positive (brighter) change greater than the threshold and is green in color. Other areas of positive and negative change that are less than the thresholds and areas of no change are black (ERDAS 2005).

Remote sensing indices were applied for the identification of environmental changes during 1984 and 2018. Two remote sensing indices were used and derived from the georectified and radiometrically calibrated Landsat TM and Landsat 8 bands. The indices used in this research were the normalized difference water index (NDWI) and the normalized difference vegetation index (NDVI) (Hadeel et al. 2011; Mishra and Prasad 2015; Mousa, 2019) and were calculated according to the following equations:

$$\text{NDWI} = (\text{NIR} - \text{MIR}) - (\text{NIR} + \text{MIR})$$

where NIR and MIR are near-infrared and middle-infrared, respectively.

$$\text{NDVI} = (\text{NIR} - \text{R}) - (\text{NIR} + \text{R})$$

where R and NIR are the red and near-infrared bands, respectively.

Finally, we used the supervised maximum likelihood classification (MLC) previously used by Salem et al. (1995) for detecting land cover classes. A maximum likelihood classification was performed with the full set of refined spectral classes when a sufficient number of spectral subclasses were acquired for all classes (Lillesand et al. 2004). MLC is considered the most effective method for supervised classification (Campbell 1987; Thomas et al. 1987). Extraction of the eleven major classes was assisted by maximum likelihood supervised classification applied to the Landsat (1984 and 2018) and planet images (2018) using field investigation information of the Tineh Plain.

Results and Discussion

Most geodiversity (geological, geomorphological) along the deltaic plains emerged from the interplay of marine, land, and river systems. Human settlements represent the result of the reciprocal influence between natural processes (geological, geomorphological) and human actions over time. In the beginning, the local geomorphological characteristics have conditioned the settlement's position (Benito-Calvo and Pérez-González 2015)—the result known here as a “geomorphosite.” According to the lifestyle of old Egyptians, they tend to construct their settlements near sources of fresh water and on elevated riverbanks to avoid floods (Parcak 2003). Over time, the more incisive anthropogenic action has reworked and reshaped the landscape, modifying the natural range of geomorphic processes (Aquaotta et al. 2018), and merged the geomorphic site and the involved antiquities, or “archeosite,” into what is called a geoarchaeomorphosite.

At the Tineh Plain (Fig. 1), the deltaic geodiversity includes the beach, the accreted coastal ridges, the Mallaha coastal lagoon, and the defunct Pelusiatic branch (associated with meandering river subenvironments). Such subenvironments represent attractive sites for old settlements, resulting in several geoarchaeomorphosites, such as those associated with the Pelusiatic branch, Tell El-Farama, Tell El-Luli, Tell El-Fadah, and Tell El-Makhzan (Fig. 1b, c).

Geomorphosites

Several geomorphosites were detected along the Tineh Plain, among are (1) the Mallaha lagoon (Figs. 1b and 2a, b); (2) the Late Holocene accretional ridges, recording the shoreline changes (Fig. 2c); and (3) the trace of the defunct Pelusiatic branch (Fig. 2e). These geomorphosites are not only restricted to such geomorphic features but also includes extensive dune fields, marshes, and sabkha areas being encountered.

The El-Mallaha lagoon (Figs. 2a, b and 3a) was a low-lying land of swamps and salt marshes that used to receive the dredged muddy sediments raised from the excavation of the Suez Canal. It occupies a large triangle area of some 56 km² with a width of 14 km at the base and narrows to 8 km at top. In the present study, the remaining area of the lagoon is only 7.3 km², representing 1.6% of the Tineh Plain (Table 1). The anthropogenic impact along the El-Mallaha lagoon was manifested with the expansion of fish breeding pans (Fig. 2a, b) and salt harvest pans (Fig. 3a) at the expense of its water body. The lagoon was subjected to continuous shrinking, being 77 km², 23 km², and 18 km² during 1984, 2003, and 2015, respectively (Kaiser 2009; Gaber et al. 2016; Arnous et al. 2017). In addition, wastewater and heavy metals dumped due to such activities may increase the lagoon's salinity and pollution. This implies that the El-Mallaha lagoon has a shallow depth, ranging from 0.15 to 0.5 m, and its salinity is much

higher than that of the Mediterranean Sea (Kaiser 2009). The Mediterranean Sea is connected to this lagoon by a small entrance near Port Fouad and other shallow tidal inlets (Frihy and Lotfy 1997). Instead of dredging the inlets and the lagoon bed to maintain seawater circulation and a suitable depth to save its biodiversity and ecosystem, the lagoon, already, was planned to become part of the New Port Said harbor.

The strand plain (Coutellier and Stanley 1987; Stanley and Warne 1998) represents another geomorphosite along the Tineh Plain; it extends from Port Fouad (west) to the city of Pelusium (east) for approximately 35 km (Fig. 1b). Its width varies considerably in an opposite trend towards the beach. It is wider to the west than to the east, being 13 km and 1 km, respectively. Eastward, it consists of bundles of low accretional beach ridges (Figs. 2c, d and 3b), with heights up to few meters, that deposited during delta progradation (Fig. 2f) and were dated back to 2000 BP (El-Asmar et al. 2015). With the development of the Tineh Plain, it is expected that the harbor project will receive several thousands of workers with its transit and industrial needs, which implies the need for the construction of a new community that supposedly will receive up to one million citizens, called New Port Said city. The location of this city is selected at the expense of the accreted ridges. A satellite image from 2018 shows that part of the city is already under construction (Fig. 2d).

Another geomorphosite is the traced location of the defunct Pelusiatic branch (Fig. 2e). The Pelusiatic branch provided direct access to the Mediterranean coast in the early 800s AD. An unusually large (~ 1 km²) and rapid influx of Nile sediments discharged possibly between 813, 816, and 820 c. AD, resulting in the accretion of an extensive strand plain (6 to 15 m thick and 35 km long, respectively, and as wide as 12 km on the subsiding delta margin). This event is possibly the reason for the blockage of sediments that filled the Pelusiatic branch and the breaking through of a new distributary to the west of present-day Port Said, probably representing the initiation of the Damietta branch (Goodfriend and Stanley 1999).

Several attempts were undertaken to trace the location of the sediments that filled the Pelusiatic branch (Sneh and Weissbrod 1973; Quintanar et al. 2013) based on the location of old settlements, like several hills or “Tel in Arabic,” including Tell El-Luli and Tell El-Fadda (Abd El-Maksoud 1984). These originated either as natural levees on an elevated overbank or as point bars or meander scars on a meander belt (Fig. 2e) with the characteristic flood plain (El-Asmar 1999; Quintanar et al. 2013). Traditionally, the historical Egyptians used such hills as secure settlements away from flood hazards and, simultaneously, to be very near to the source of Nile water. Such sites offered an ideal location to exploit both riverine and maritime transportation routes through trade and regional floral and faunal resources for hunting, fishing,

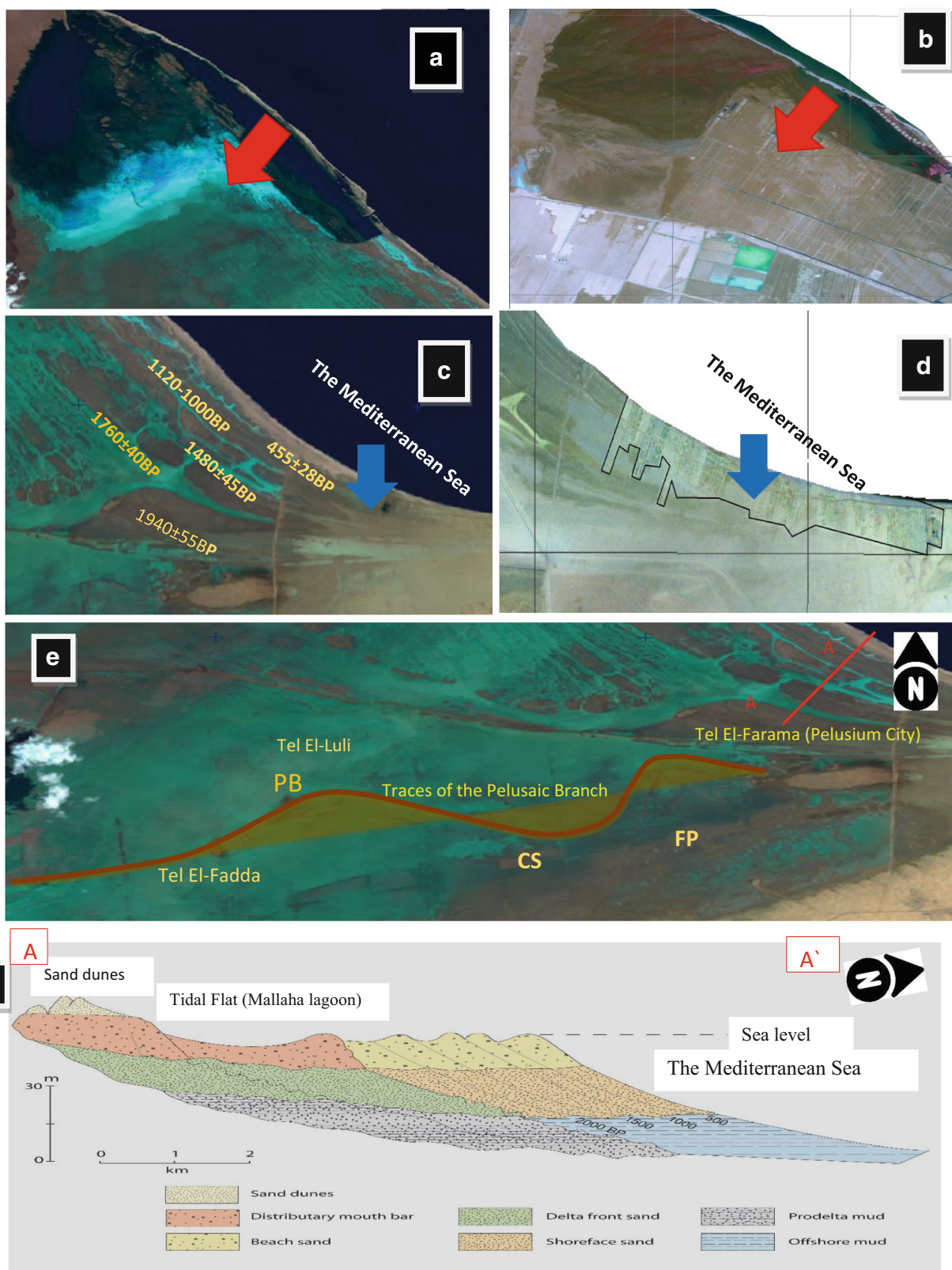


Fig. 2 Correlation of satellite images of 2018 (a) and 1984 (b) showing the expansion of the fish farm area (red arrow) at the expense of the lagoon and the surrounding wetlands. The geomorphosites, the accreted coastal ridges, related to shorelines dating back to Late Holocene age between c. 2000 BP and 500 BP (50 BC to 1450 AD) (c) during 1984, while in 2018 (d) a new

city was under construction (blue arrow). The geomorphosite trace of the Pelusiac branch through the geomorphic features associated with the meander stream belt including the muddy flood plain “FP,” crevasse splay “CS,” and point bar sands “PB” (e), cross section A-A’(e) showing the deltaic progradation and the accreted costal ridges (f).

cultivation, and animal husbandry (Parcak 2003; Benito-Calvo and Pérez-González 2015).

Not only the Pelusiatic branch on the eastern border of the Nile Delta but also a natural boundary of dunes covers the deltaic plain and running SW-NE (Fig. 3c). The difference between the high dune and the nearly sea level delta plain may be related to active structure (Neev 1977), which was mapped and identified as a major strike-slip fault (Fig. 1a) trending NE-SW, bordering the eastern Nile Delta, known as the Pelusium fault line (Neev et al. 1985). The delta front and mouth bar sands characterized the deltaic plain (Fig. 3d, e) and the classical beach with the characteristic heavy minerals concentrated as black parallel laminae, indicating different stages of erosion/accretion (Fig. 3f).

Geoarcheomorphosites

The deltaic plain comprises most of the discovered geoarcheomorphosites. The city of Pelusium, “Tel El-Farama in Arabic” (Fig. 4), represents one of the geoarcheomorphosites. The city of Pelusium’s ancient name, coming from the Greek pelos for mud or silt, reflects its location. The city and the surroundings existed during Egypt’s Late Dynastic Kingdom (Stanley 2005). Its history begins after the Persian invasions of Egypt, from approximately the sixth c. BC in Egypt’s Late Period (Manley 1996). During 640 AD and the Arabic conquest, the city was in a coastal position (Goodfriend and Stanley 1999). The accounts of Al-Makrizi in the fifteenth c. AD indicated that the sultan El-Moutawakel built

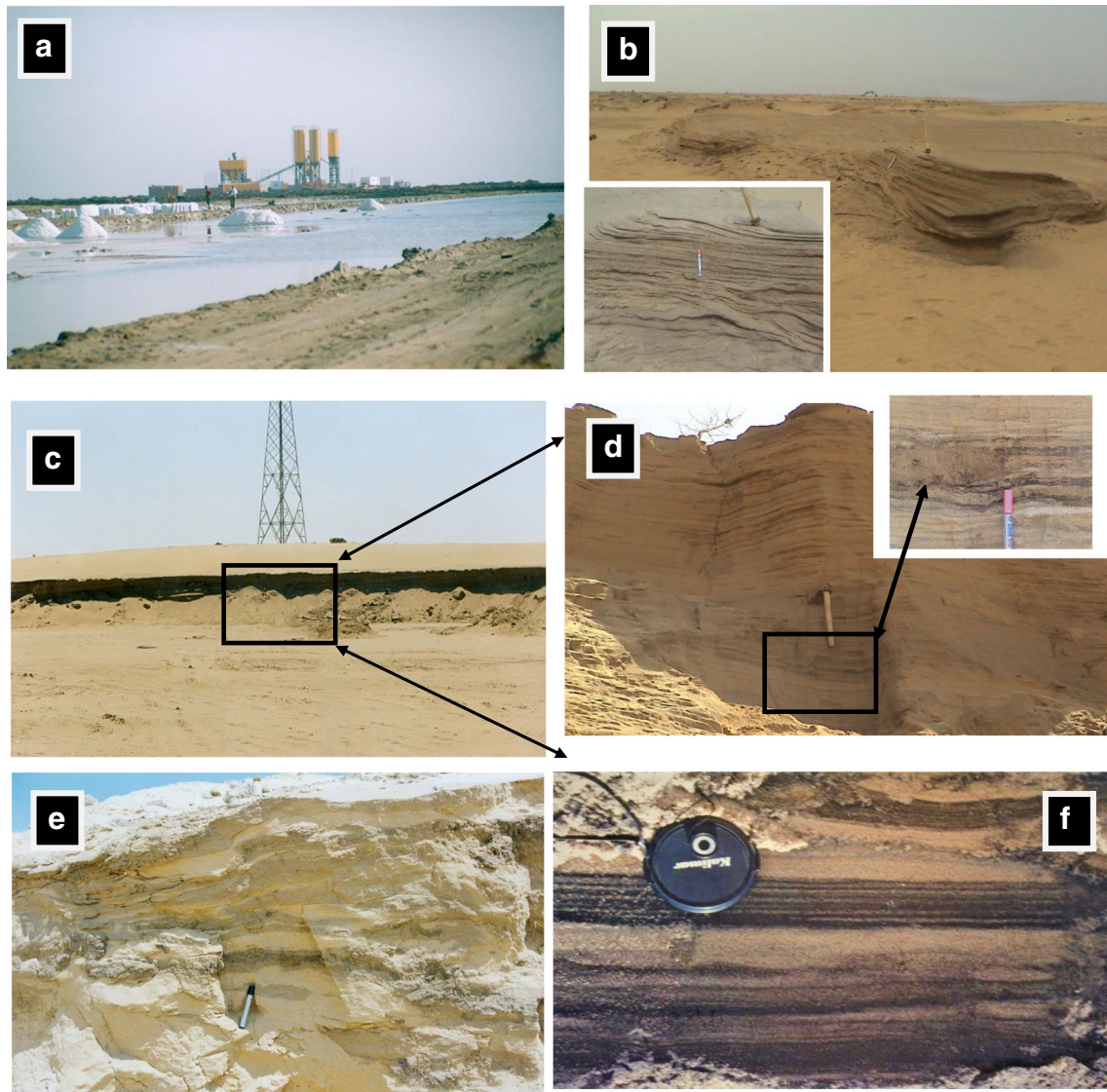


Fig. 3 Geodiversity along the Tineh Plain, the Mallaha lagoon where salts mineralized (a). Close-up of part of the accreted coastal ridges with tabular horizontal stratification (b). Sand dune covers the deltaic plain (c). Close-up of the delta front sediments exhibiting planar cross stratification with the characteristic rippled bioturbated sands intercalated with thin

mud laminae (d). The distributary moth bar sand with the characteristic bifurcated flaser bedding of muddy sand (< 5% mud) (e). The beach with the characteristic heavy minerals concentrated in black parallel laminae, indicating different stages of erosion/accretion (f)

Table 1 The area of the different land covers for 1984 and 2018 derived from ISODATA classification method

Class name	Area 1984 (km ²)	Percentage (%)	Area 2018 (km ²)	Percentage (%)
Accreted sandy ridge	128.6	20.3	30	4.7
Salt crust	141	22.3	65	10.3
Wetland and sabkha	31.2	4.9	16 + 40	2.5 + 6.3
Sand dune	75	11.8	60	9.4
Deltaic clay	124	19.6	35	5.5
Sand fill	–	–	32.2	5
Fish farm	–	–	100	15.8
Agriculture	–	–	112	17.7
Mallaha lagoon	77	12	7.3	1.6



Fig. 4 The archeosites at the Great Pelusium showing the Gatehouse to Pelusium's sixth-century AD fortress (a), the Pelusium citadel wall (b), the water canals of Roman baths (c), Roman pillars (d), the Byzantine church (e), and the Roman amphitheater (f) at Tell El-Makhzan, the city of Pelusium

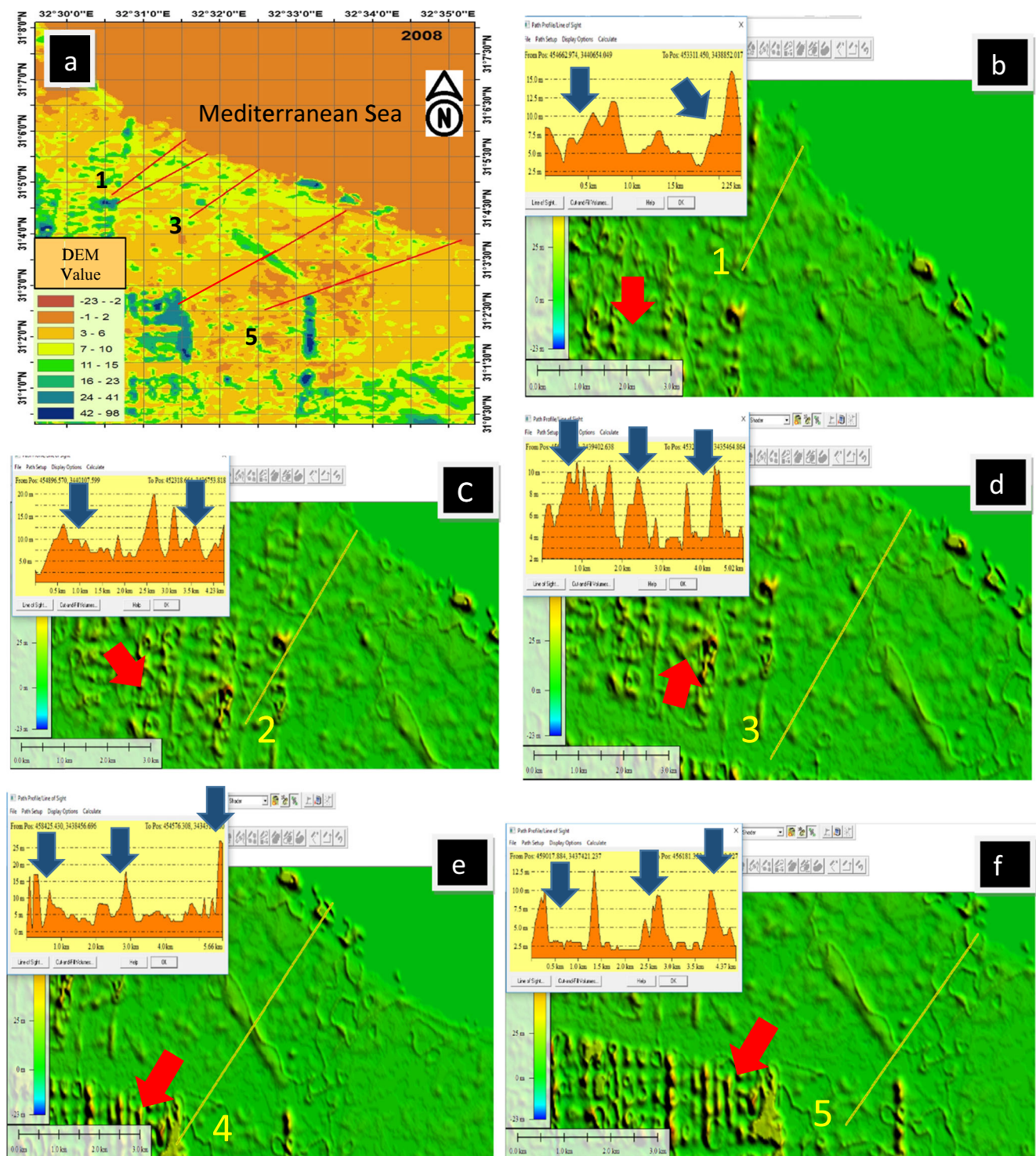


Fig. 5 Five profiles (a) for digital elevation model (DEM, 2008) each profile from 1 to 5 (b–f) showing at least three groups (blue arrows, inside boxes, b–f) of coastal ridges running parallel to the shoreline having elevation between 5 and 15 m above sea level such ridges record the

Late Holocene shoreline changes (b–f), the advancement of urbanization and fish breeding farms (red arrows, b–f) represent hazards on the geodiversity of this area

fortifications in the region in 853–854 AD and Al-Ya’akubi found the strand plain already in existence when he visited the area in the late 800 AD (Bouriant 1900). This is interpreted as

the strand plain being in existence during the 853–854 AD and the present-day coast having formed since the fifteenth c. AD. This is in accordance with the conclusion of Goodfriend and

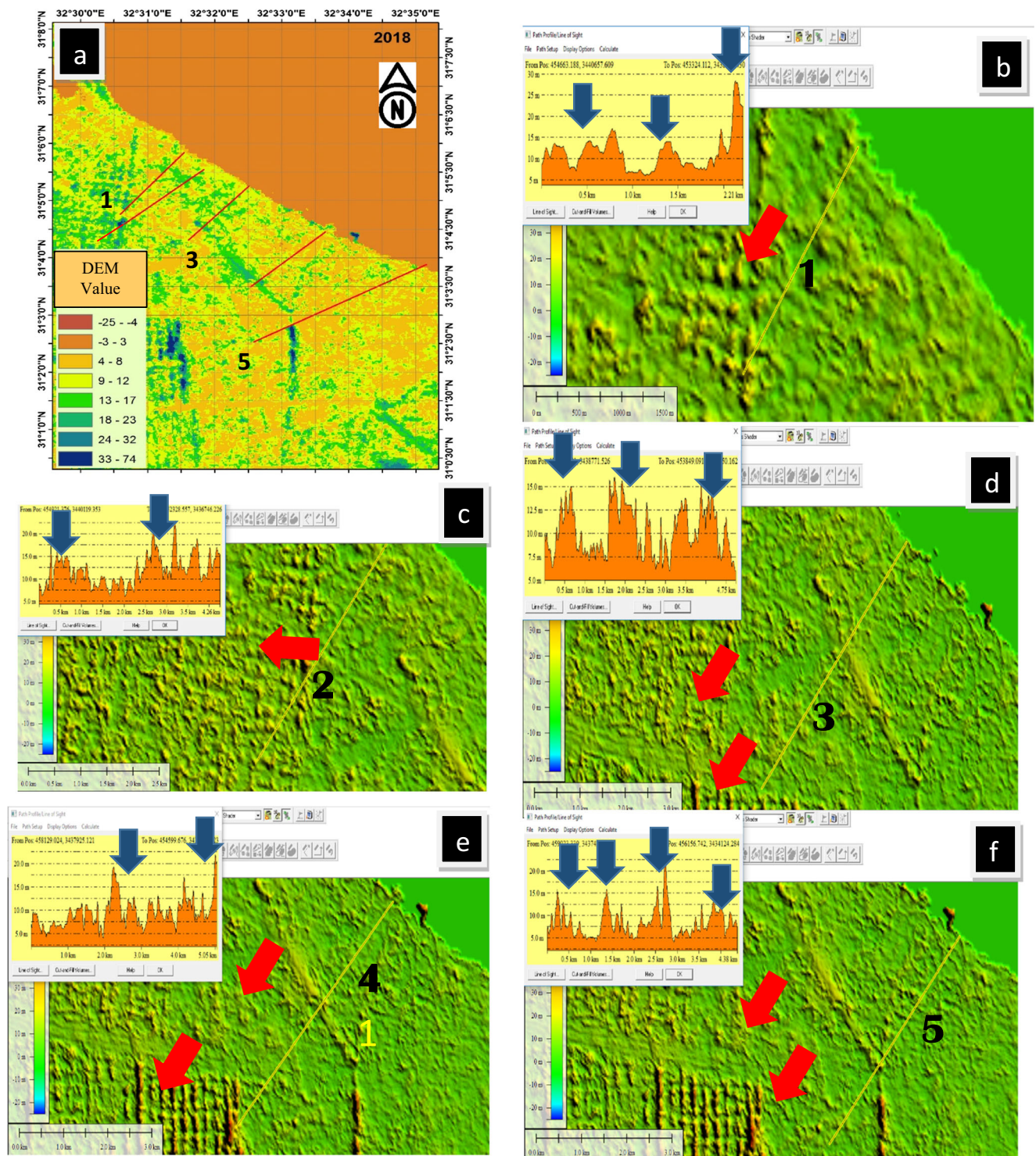


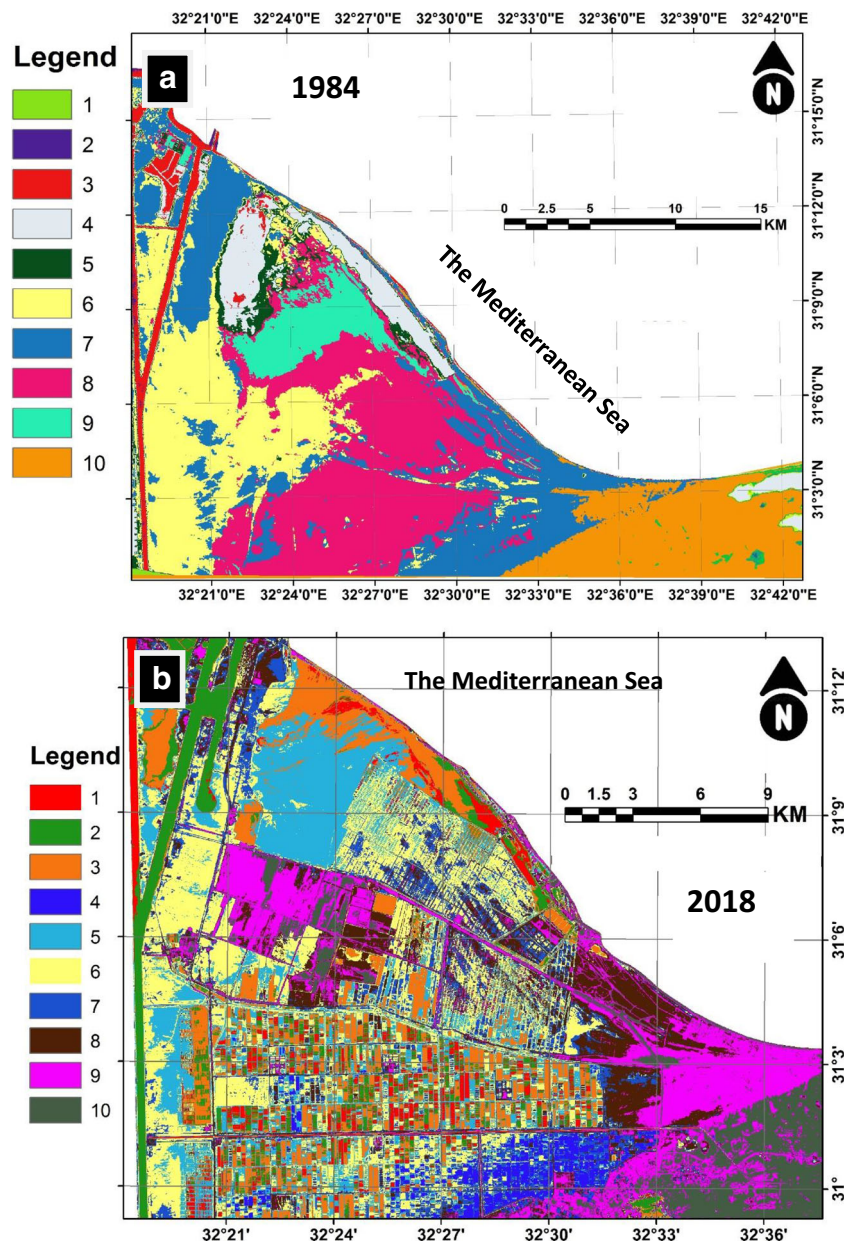
Fig. 6 Five profiles (a) for digital elevation model (DEM, 2018) and each profile from 1 to 5 (b–f) showing changes on the elevation along the coastal ridges from 10 to 28 m (look inside boxes, blue arrows) above

sea level due to drilling and dredging activities for urban constructions, roads, and fish breeding as well as farm expansion (red arrows, b–f) which threaten the geodiversity and archaeological sites

Stanley (1999) who indicated that the strand plain with the accreted ridges developed due to strong successive floods in 813, 816, and 820 AD. The radiocarbon dates support this view and

indicate ages of 455 ± 28 BP for the present coast, while the strand plain formed between 1760 ± 40 BP and 1120 ± 45 BP (El-Asmar et al. 2015), between the third and ninth c. AD.

Fig. 7 Unsupervised classification of satellite images representing the Tineh Plain showing more than 15 classes and how the plain is suffering from dramatic anthropogenic changes from 1984 (a) to 2018 (b)



After Israel’s withdrawal from Sinai in 1982, huge excavations began by the inspectors of the Supreme Council of Antiquity in collaboration with different foreign missions. Perhaps the most spectacular find was the wall, gates, and Roman bath (Fig. 4a, b, c) with polychrome mosaic floors in geometric designs that dated back to the third c. AD (Abd El-Maksoud 1984). In 1991, new discoveries were made, including the Byzantine church (Fig. 4d, e) and the Roman amphitheater (Fig. 4f) that belong to the fifth and sixth c. AD at Tell El-Makhzan (Abd El-Samie 1992; Bonnet and Abd El-Samie 2004; Bonnet et al. 2004, 2010) with the characteristics of Roman pillars (Fig. 4d). Ibrahim et al. (1998) made shallow geophysical investigations in the city of Pelusium in order to locate the buried archeological remains. They found that the

magnetic method was more successful than the electric resistivity method in locating the buried antiquities made of fired bricks, which have high magnetic susceptibility and remnant magnetism relative to the surrounding clayey soils. The city of Pelusium was crossed by the Holy Family’s journey in Egypt, but they did not stay for a long time. They were very scared to stay in a border city, which explains the exclusion of the Pelusium from the eight Egyptian locations on the Vatican’s pilgrimage list (Tarek Al-Hussaini, personal communication).

Besides the negative impact and results due to corrosion of the building stones and mortars and plasters due to the prevailed environmental conditions (2019), the human expansion, expressed in different forms of urbanization, industrial, logistical, agricultural, and fish breeding, may represent

additional potential hazards on the geoarcheomorphosites. A plan for conservation should be implemented in the form of sustainable development to save a great part of history and geoheritage of Egypt. The Ministry of Tourism is invited to offer smart applications regarding such coastal heritage sites (Almobaideen et al. 2016; Taha and El-Asmar 2019) to allow tourism to fix on their programs when they visit Egypt. The promotion of these heritage sites near the beaches supports cultural tourism as well as recreational tourism.

Remote Sensing Application

Unfortunately, during the early generation of the satellite images, no DEM data had been issued. The DEM for this study was applied for selected profiles during 2008 (Fig. 5) and 2018 (Fig. 6). The DEM profiles of 2008 reflect tremendous anthropogenic changes deduced from changes in elevation and the number of accreted sand ridges. At least three groups of coastal ridges (Fig. 5) run parallel to the shoreline having elevations between 5 and 15 m above sea level; such ridges record Late Holocene shoreline changes between 2000 and 500 BP triggered by successive floods dating back to the eighth c. AD (Goodfriend and Stanley 1999). However, clues

for some anthropogenic activities are more apparent (Fig. 5), including roads, and fish and agricultural farms.

However, the DEM profiles of 2018 (Fig. 6) show changes in elevation along the coastal ridges from 10 to 28 m above sea level. Such changes resulted from the land filling of depressions between the accreted ridges and the paving of roads. The DEM profiles also show an expansion of anthropogenic activities in the form of fish farms and agricultural lands. Such expansions represent strong pressure threatening the archeosites. At present, there is a plan for construction of a new 55-km² residential project (Fig. 2d), of which 3 km² is under construction. The new city will be entirely constructed at the expense of the accreted ridges.

In general, the unsupervised classification of LU/LC applied on the satellite images of 1984 and 2018 reflects more than 20 classes (Fig. 7). The image of 2018 appears dramatically changed relative to that of 1984, which explains to what extent this change in LU/LC was significant. The difference map (Fig. 8) is a change detection map that resulted from the digital subtraction of the geologic features of 1984 from that of 2018. The unchanged areas appear in black, while the red color indicates low reflection due to water advance compared with high land reflection, which appears in a green-yellow

Fig. 8 Change detection map that resulted from the difference between the satellite images of 1984 and 2018; the positively added areas appear in green while the negatively induced lost areas appear in red. The unchanged areas appear in black. The area surrounding the archeosites at the Great Pelusium (yellow rectangle) appears to have completely changed with the expansion of anthropogenic activities, such as fish and agricultural farms, threatening the archeosites (yellow arrows)

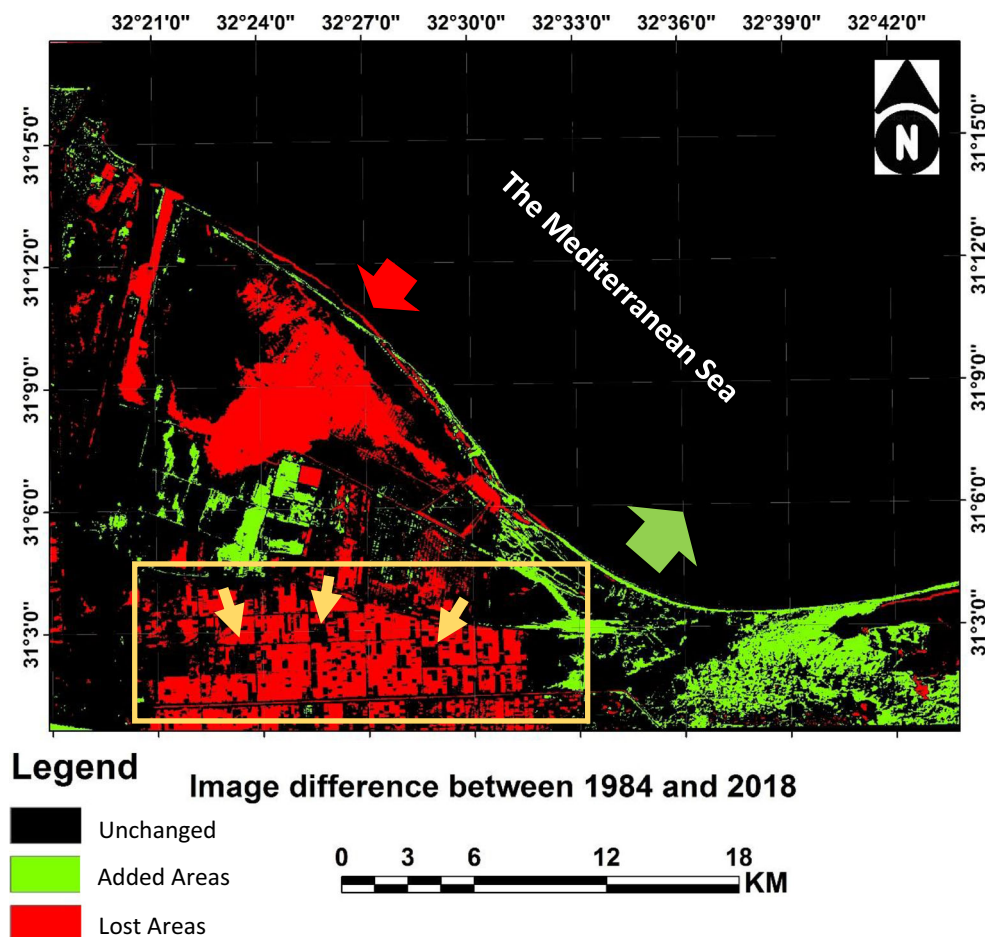


Fig. 9 Normalized difference water index (NDWI) showing the aerial changes between water and land during 1984 (a) and 2018 (b)

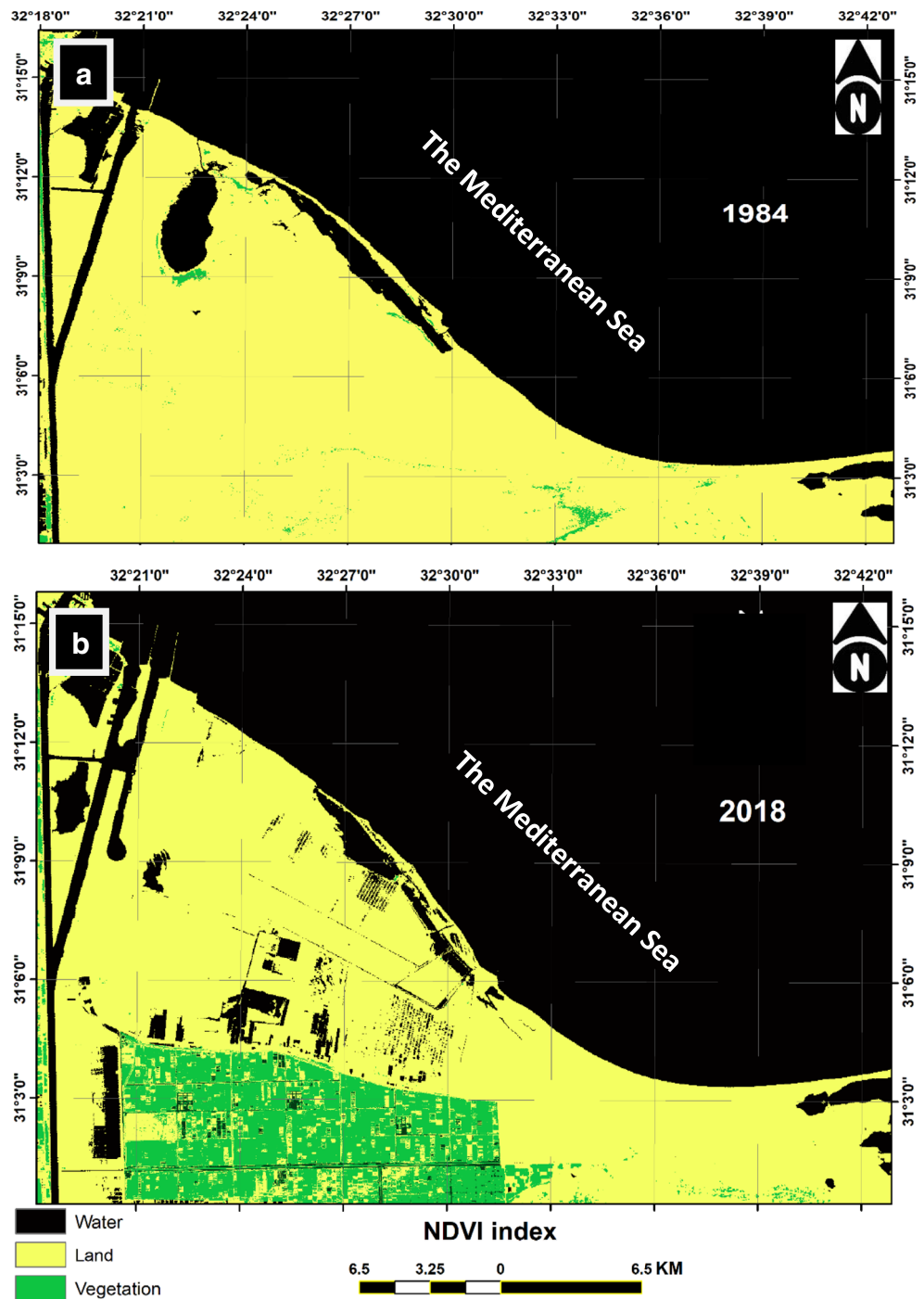


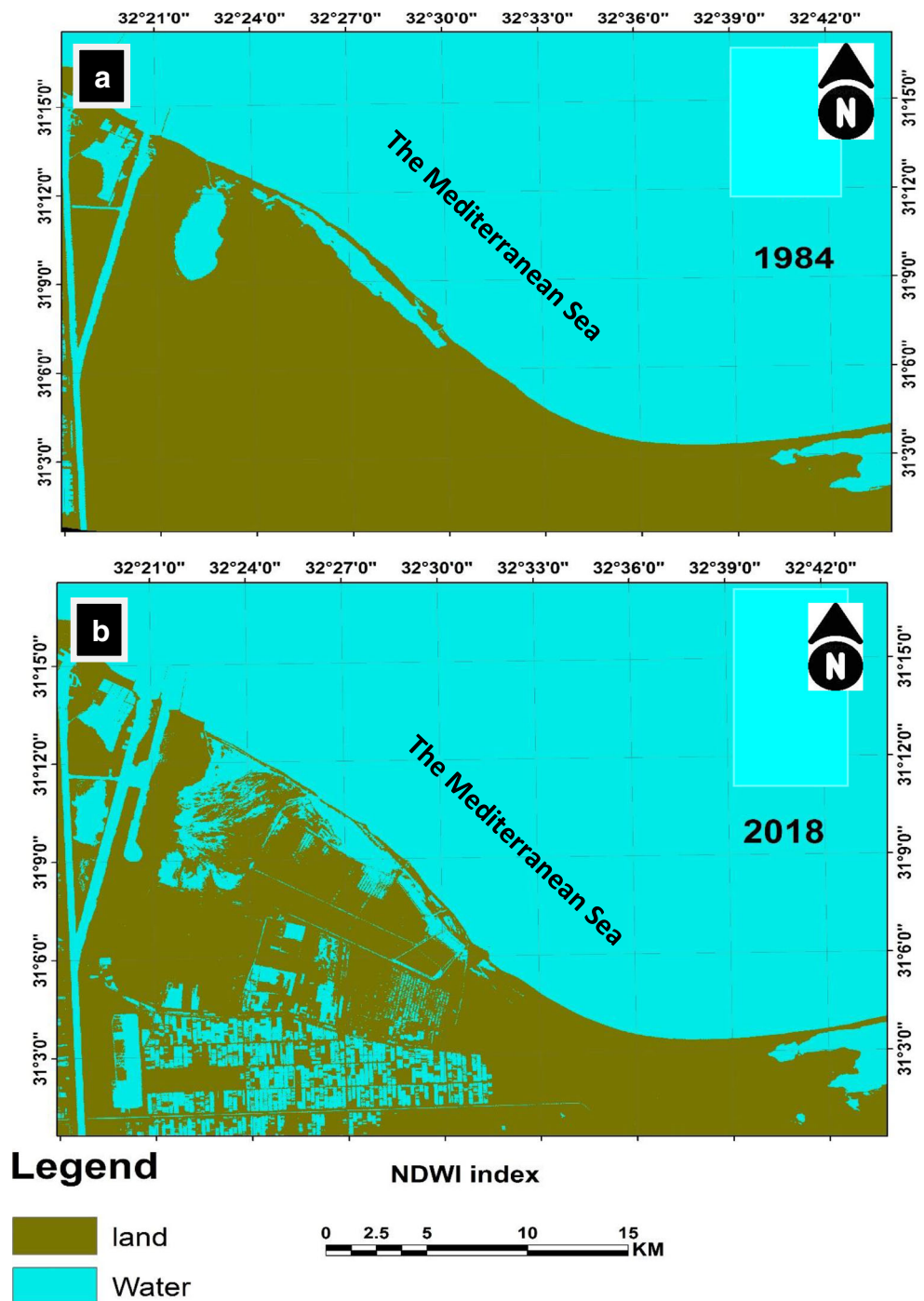
Table 2 The area of the different land covers for 1984 and 2018 derived from remote sensing indices

Index name	Class cover	Area 1984 (km ²)	(%)	Area 2018 (km ²)	(%)
NDVI	No vegetated land	615.5	97.3	517	81.8
	Vegetation	16.5	2.6	115	18.2
	Total	632	100	632	100
NDWI	Dry lands	551	87.2	473	74.8
	Water bodies and wetlands	81	12.8	159	25
	Total	632	100	632	100

color. The expansion of the red color supports the increase in areas of fish farms and agriculture activities at the expense of the geomorphosites of the accreted ridges, sabkhas, and lagoon areas (Fig. 8; Table 1). The fish farms appear to surround geoarcheomorphosites, such as Tell El-Luli and Tell El-Fadda (Figs. 1b, c and 8), which represent point bars and crevasse splays of the defunct Pelusiatic branch and part of the old settlements during the fifth c. BC (Figs. 2e and 4).

The NDVI index was applied on both satellite images of 1984 and 2018 (Fig. 9) to distinguish land, water, and vegetation. The vegetation in the study area was 16.5 km² (Fig. 9a) during 1984 and represented 2.6% of the study area, whereas during 2018 (Fig. 9b), the vegetated area increased by approximately 18.2% to reach 115 km² (Table 2). The non-vegetated land was 615.5 km², representing 97.3% of the study area, during 1984, whereas during 2018, it decreased to 517 km², representing 81.8% (Table 2).

Fig. 10 Normalized difference vegetation index (NDVI) showing the aerial changes between water, land, and vegetation during 1984 (a) and 2018 (b)



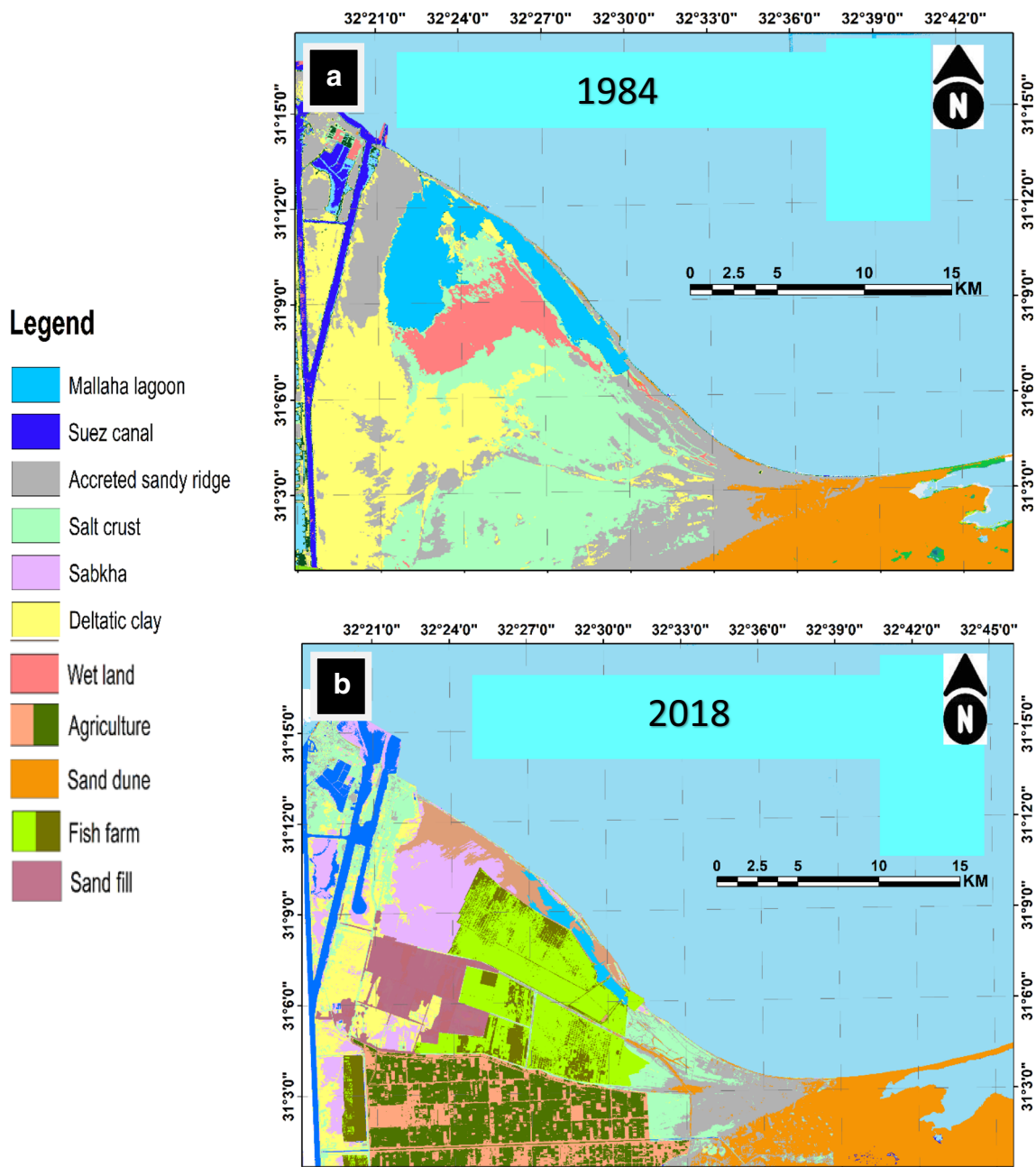


Fig. 11 Supervised classification of satellite images from 1984 (a) and 2018 (b) showing nine classes that changed due to different anthropogenic activities, such as the expansion of agricultural land, fish

farms, and other urbanized areas that represent great pressure and human impact hazards on the geoarcheomorphosites

To distinguish water bodies from wetland and fish farms more accurately, the normalized difference water index (NDWI) was used to construct NDWI maps for 1984 and 2018 (Fig. 10). The dry land area was 551 km², representing 87.2% of the study area, during 1984 (Fig. 10a; Table 2) and was 473 km², representing 74.8% of the study area, in 2018 (Fig. 10b; Table 2). The water bodies and wetlands occupy an area of approximately 81 km², representing 12.8% of the study area, during 1984 (Fig. 10a; Table 2) and increased by 2018 to 159 km², representing 25% of the study area (Figs.

10b and 11; Table 2). Such an increase in the water bodies and wetlands was mostly due to the expansion of fish farms that occupied 100 km² and 15.8% of the study area (Table 2). The calculated vegetation or agricultural area appears similar in both methods the (ISODATA) unsupervised classification and NDVI map ranging between 112 and 115 km², respectively, and water bodies and wetlands equal to 159 km², of which 100 km² is related to fish farms.

The field verification allowed us to produce the supervised classification and reduce the classes to nine (Fig. 11). Table 1

shows changes in the areas of the total classes and documents the changes detected from the satellite images. In 1984, the detected classes include accreted ridges (128.6 km²), wetland and sabkhas (31.2 km²), sand dunes (75 km²), and deltaic clays (124 km²), representing 20.3, 22.3, 4.9, 11.8, and 19.6%, respectively. In 2018, the same classes became 30, 65, 56, 60, and 35 km², representing 4.7, 10.3, 8.8, 9.4, and 5.5%, respectively. Such reduction in the class areas comes at the expense of the expanded areas of sand fill (32.2 km² of 5%), fish farms (100 km² of 15.8%), and agriculture land (112 to 115 km² of 17.7%) (Table 1).

Conclusions

Most of the geodiversity observed along the deltaic plains are due to the interplay of marine, land, and river systems. Such interactions resulted in the emergence of geomorphosites. Recently, the anthropogenic factor became an additional factor that played an important role in transforming and reshaping the geomorphosite to a geoarcheomorphosite.

This study records the geomorphosites related to the deltaic subenvironments along the Tineh Plain. Among them are the Mallaha lagoon, the accreted beach ridges that record the shoreline history during the last 2000 BP, and the traces of the old defunct Pelusiac branch (eighth c. AD) of the Nile, which was described as a meandering stream with the characteristic flood plains, natural levees, crevasse splays, and point bars. These geomorphic features attracted the old Egyptians to construct their settlements very near to the water source for agricultural and fishing purposes and away from the hazards of flash floods. Such settlements documented the old Pelusiac branch of the Nile and the Great Pelusium (Tell El-Farama) archeosites (third to fifth c. AD).

Quantification of the potential risk resulting from anthropogenic activities shows how much the Tineh Plain is at risk. The area of geoarcheomorphosites along the Tineh Plain during 1984 was 424.8 km², representing approximately 67.1% of the plain, in addition to sand dune area of 75 km², representing 11.8%. This area was occupied by fish and agricultural farms and an urban expansion that reached 244.2 km² during 2018, representing 38% of the Tineh Plain. The construction of a part of a new hub in the Suez Canal corridor, in an area of 164 km² representing 30.3% of the plain, will add more pressure to the geoarcheomorphosites. A conservation plan should be implemented in the form of sustainable development to save an important part of the history and geoheritage of Egypt.

Acknowledgments The authors thank the Deanship of Scientific Research and the Researchers Support and Services Unit at King Saud University for their technical support.

Funding Information This study was financially supported by the Deanship of Scientific Research at King Saud University through Research Group No. RG-1439-061.

References

- Abd El-Maksoud M (1984) Preliminary report on the excavation of tell el-Farama (Pelusium) first two seasons (1983/84 and 1984/5). *ASAE* 70:3–8
- Abd El-Samie M (1992) Preliminary report on the excavations at tell el-Makhzan (Pelusium). *CRIPEL* 14:91–95
- Almobaideen W, Allan M, Saadeh M (2016) Smart archaeological tourism: contention, convenience and accessibility in the context of cloud-centric IoT. *Mediterranean Archaeology and Archaeometry* 16(1):227–236. <https://doi.org/10.5281/zenodo.35535>
- Arnous MO, El-Rayes AE, Helmy AM (2017) Land-use/land-cover change: a key to understanding land degradation and relating environmental impacts in northwestern Sinai, Egypt. *Environ Earth Sci* 76:263–221. <https://doi.org/10.1007/s12665-017-6571-3>
- Aquaotta F, Faccini F, Fratianni S, Paliaga G, Sacchini A (2018) Rainfall intensity in the Genoa Metropolitan Area (Northern Mediterranean): secular variations and consequences. *Weather*. <https://doi.org/10.1002/wea.3208>
- Belen Castro M (2015) A historical review of the Egyptian calendars: the development of time measurement in ancient Egypt from Nabta Playa to the Ptolemies. *Sci Cult* 1(3):15–27. <https://doi.org/10.5281/zenodo.18446>
- Bonnet C, Abd El-Samie M (2004) Les églises de tell el-Makhzan. La campagne de fouille 2002, avec Une annexe de D. Dixneuf, « La céramique romaine tardive et byzantine de tell el-Makhzan. L'église méridionale et l'aire funéraire. Observations préliminaires, CRIPEL 24:5–45
- Bonnet C, Abd El-Samie M, El-Tabai A (2004) L'église cruciforme tétraconque de Farama Sud à Péluse (Egypte). *L'archéologue* 73: 31–33
- Bonnet C, El-Tabai A, Carrez-Maratray JY, Abd El-Samie M (2010) Le temple romain, les bains et l'église tétraconque des faubourgs de Farama à Péluse (Nord Sinai). *Genava* 58:142–163
- Bouriant U (1900) Maqrizi: description Topographique et Historique de l'Egypte (part II) [translation of the 14th century Arabic work]. *Mémoires Publiés par les Membres de la Mission Archéologique Française du Caire* 17:371–748
- Butler AJ (1996) The Arab conquest of Egypt and the last thirty years of Roman dominion (in Arabic). Madbouli Press, Cairo, Trans. M.F. Abu Hadid
- Campbell JB (1987) Introduction to remote sensing. The Guilford Press
- Chen H, Ye S, Zhang D, Zhang D, Areshkina L, Ablameyko S (2018) Change detection based on difference image and energy moments in remote sensing image monitoring. *Pattern Recognit Image Anal* 28: 273–281
- Coutellier V, Stanley DJ (1987) Late Quaternary stratigraphy and paleogeography of the eastern Nile Delta, Egypt. *Mar Geol* 77:257–275
- Drury SA (2001) Image interpretation in geology. Nelson Thornes Blackwell Science, Cheltenham Malden 290
- El-Asmar HM (1999) Late Holocene stratigraphy and lithofacies evolution of the Tineh plain northwestern corner of Sinai. *Egypt Egypt J Geol* 43(2):119–134
- El-Asmar HM, Taha MMN, El-Kafrawy SB, El-Sorog AS (2015) Control of Late Holocene geo-processes on the sustainable development plans of the Tineh plain, NW Sinai coast, Egypt. *J Coast Conserv* 19:141–156. <https://doi.org/10.1007/s11852-015-0377-9>
- El-Asmar H, Taha MMN, El-Sorogy AS (2016) Morphodynamic changes as an impact of human intervention at the Ras El-Bar-Damietta

- Harbor coast, NW Damietta promontory, Nile Delta, Egypt. *J Afr Earth Sci* 124:323–339
- ENVI (2009) Atmospheric correction module: QUAC and FLAASH user's guide.
- EPM (2014) Master plan for Port Said East Port <http://epmcon.com/article/23883/Master-Plan-For-Port-Said-East-Port>
- ERDAS (2005) Field guide. Leica Geosystems Geospatial Imaging, LLC
- Fernández JF, Alonso DA, González PA (2016) GIS and geoarchaeological analysis in superficial open-air sites: the case of Raña de Cañamero Neanderthal settlement (Guadiana Basin, Spain). *Mediterr Archaeol Archaeom* 16(2):47–59
- Foody G (2003) Remote sensing of tropical forest environments: towards the monitoring of environmental resources for sustainable development. *Int J Remote Sens* 24:4035–4046
- Frihy OE, Lawrence D (2004) Evolution of the modern Nile Delta promontories: development of accretional features during shoreline retreat. *J Environ Geol* 46:914–931
- Frihy OE, Lotfy MF (1997) Shoreline changes and beach-sand sorting along the northern Sinai coast of Egypt. *Geo-Mar Lett* 17:140–146
- Gaber A, Geriess MH, Shaheen S, El-Fattah MA (2016) Mapping the surface changes in the area of east port-said, Egypt using multi-temporal and multi-sensors remote sensing data. *IOSR J App Geol Geophy (IOSR-JAGG)* 4(5):19–29
- GAFI (2014) MEGA projects integrate development at the center of the of the Suez Canal. <http://www.mfa.gov.eg/MFANews/NewsArabic/Documents/Mega%20Projects%2023-1-2013.pdf>
- Gamba P, Dell'acqua F, Houshmand B (2003) Comparison and fusion of LiDAR and InSAR digital elevation models over urban areas. *Int J Remote Sens* 24(22):4289–4300. <https://doi.org/10.1080/0143116031000096005>
- Goodfriend GA, Stanley DJ (1999) Rapid strand-plain accretion in the northeastern Nile Delta in the 9th century AD and the demise of the port of Pelusium. *Geology* 27:147–150
- Hadeel A, Jabbar M, Chen X (2011) Remote sensing and GIS application in the detection of environmental degradation indicators. *Geo-spat Inf Sci* 14(1):39–47
- Herold M, Scepan J, Clarke KC (2002) The use of remote sensing and landscape metrics to describe structures and changes in urban land uses. *Environ Plan* 34:1443–1458
- Hussain M, Chen D, Cheng A, Wei H (2013) Change detection from remotely sensed images: from pixel-based to object-based approaches. *ISPRS J Photo Remote Sens* 80:91–106
- Ibrahim EH, Sherief MR, Al-Metwally AA (1998) Shallow geophysical investigations on tell el Farama, Northwest Sinai. *Egypt Archaeol Prospect* 5:91–100
- Kaimaris D (2018) Ancient theaters in Greece and the contribution of geoinformatics to their macroscopic constructional features. *Sci Cult* 4(3):9–25. <https://doi.org/10.5281/zenodo.1409800>
- Kaiser M (2009) Environmental changes, remote sensing, and infra structure development: the case of Egypt's East Port Said harbour. *Appl Geogr* 29:280–288
- Lillesand TM, Kiefer RW, Chipman JW (2004) Remote sensing and image interpretation. John Wiley & Sons 763
- Lu D, Mausel P, Brondizio E, Moran E (2004) Change detection techniques. *Int J Remote Sens* 25:2365–2404
- Manley B (1996) Historical atlas of ancient Egypt. Penguin Books, London, p 144
- Mather PM (1999) Computer processing of remotely-sensing images, an introduction (2nd ed.). Chichester: John Wiley and Sons, pp. 1–75.
- Memarsadeghi N, Netanyahu NS, LeMoigne J (2007) A fast implementation of the ISODATA clustering algorithm *Int J Comp Geom App*
- Mishra K, Prasad P (2015) Automatic extraction of waterbodies from Landsat imagery using perceptron model. *J Comp Env Sci*:1–8
- Monterroso-Checa A (2017) Remote sensing and archaeology from Spanish Lidar-PNOA: identifying the amphitheater of the Roman city of Torreparedones (Córdoba-Andalucía-Spain). *Mediterr Archaeol Archaeom* 17(1):15–22. <https://doi.org/10.5281/zenodo.258079>
- Mousa AB (2019) Monitoring building materials exposed to marine environment: examples from Farasan Islands. *Saudi Arabia Sci Cult* 5(2):7–20
- Neev D, (1977) The Pelusium line—a major trans-continental shear. *Tectonophysics* 38(3–4), T1–T8
- Neev D, Greenfield L, Hall JK (1985) Slice tectonics in the Eastern Mediterranean Basin. In: D.J. Stanley and F.C. Wezel (Editors), *Geological Evolution of the Mediterranean Basin*. Springer, New York N.Y., pp.249–269
- Parcak SH (2003) Archaeological evidence for abrupt climate change: results from satellite imagery analysis and subsequent ground truthing in the El-Manzalah region, Northeast Egyptian Delta. <http://adsabs.harvard.edu/abs/2003AGUFMPP22C..03P>
- Pennington BT, Bunbury JM, Hovius N (2016) Emergence of civilisation, changes in fluvio-deltaic styles and nutrient redistribution forced by Holocene Sea-level rise. *Geoarchaeology* 31(3):194–210
- Pennington BT, Sturt F, Wilson P, Rowland J, Brown AG (2017) The fluvial evolution of the Holocene Nile Delta. *Quaternary Sci Rev* 170: 212–231
- Quintanar J, Khan S, Fathy MS, Zalut AAM (2013) Remote sensing, planform, and facies analysis of the plain of Tineh, Egypt for the remains of the defunct Pelusiac River. *Sediment Geol* 297:16–30
- Rashad HM, Abdel-Azeem AM (2010) Lake Manzala, Egypt: a bibliography. *Assiut Univ J Botany* 39(1):253–289
- Sabins FF (1997) Remote sensing principles and interpretation. H. Freeman Company, New York, pp 366–371
- Salem BB, El-Cibahy A, El-Raey M (1995) Detection of land cover classes in agro ecosystems of northern Egypt by remote sensing. *Int J Remote Sens* 16(14):2518–2594
- Sestini G (1989) Nile delta: a review of depositional environments and geological history. In: Whateley MKG, Pikerling KT (eds) *Deltas: sites and traps for fossil fuels*, 41. Geological Society Special Publication, Blackwell Scientific Publications, pp 99–127
- Shalaby A, Tateishi R (2007) Remote sensing and GIS for mapping and monitoring land cover and land-use changes in the northwestern coastal zone of Egypt. *Appl Geogr* 27:28–41
- Sneh A, Weissbrod T (1973) Nile delta: the defunct Pelusiac branch. *Science* 180:59–61
- Sneh A, Weissbrod T, Perath I (1975) Evidence for ancient Egyptian frontier canal. *Am Sci* 63:543–548
- Srivastava PK, Han D, Rico-Ramirez MA, Bray M, Islam T (2012) Selection of classification techniques for land use/land cover change investigation. *Adv Space Res* 50(9):1250–1265
- Stanley DJ (2005) Submergence and burial of ancient coastal sites on the subsiding Nile delta margin, Egypt. *Méditerranée* 1(2):65–73
- Stanley DJ, Toscano M (2009) Ancient archaeological sites buried and submerged along Egypt's Nile Delta coast: gauges of Holocene Delta margin subsidence. *J Coast Res* 25(1):158–170
- Stanley DJ, Warne AG (1993) Nile delta, recent geological evolution and human impact. *Science* 260:628–634. <https://doi.org/10.1126/science.260.5108.628>
- Stanley DJ, Warne AG (1998) Nile delta in its destruction phase. *J Coast Res* 14:794–825
- Stanley DJ, Bernasconi MP, Jorstadt TF (2008) Pelusium, an ancient port fortress on Egypt's Nile Delta coast: its evolving environmental setting from foundation to demise. *J Coast Res* 24(2):451–462
- Taha MMN, El-Asmar HM (2019) Geo-archaeological sites are at risk, the Manzala lagoon, NE Nile Delta coast, Egypt. *Geoheritage* 11: 441–457. <https://doi.org/10.1007/s12371-018-0297-9>
- Thomas IL, Benning VM, Ching NP (1987) Classification of remotely sensed images. Adam Hilger, Bristol
- Yuan J, Niu Z (2008) Evaluation of atmospheric correction using FLAASH. In *IEEE international workshop on earth observation*

- and remote sensing applications. EORSA: 1–6. Beijing. <https://doi.org/10.1109/eorsa.2008.4620341>
- Yuan F, Sawaya KE, Loeffelholz BC, Bauer ME (2005) Land cover classification and change analysis of the twin cities (Minnesota) metropolitan area by multitemporal Landsat remote sensing. *Remote Sens Environ* 98:317–328
- Zaafarany N, Alsahar S (2014) The prospects of developing Suez Canal region- a futuristic vision. Vienna 10th International Academic Conference.